Colloids and Surfaces B: Biointerfaces 111 (2013) 162–170

Contents lists available at SciVerse ScienceDirect

Colloids and Surfaces B: Biointerfaces

journal homepage: www.elsevier.com/locate/colsurfb

Synthesis, characterization and applications of carboxylated and polyethylene-glycolated bifunctionalized InP/ZnS quantum dots in cellular internalization mediated by cell-penetrating peptides

Betty R. Liu[a], Jeffrey G. Winiarz[b], Jong-Sik Moon[b], Shih-Yen Lo[c], Yue-Wern Huang[d,**], Robert S. Aronstam[d], Han-Jung Lee[a,*]

[a] Department of Natural Resources and Environmental Studies, National Dong Hwa University, 1, Sec. 2, Da-Hsueh Road, Shoufeng, Hualien 97401, Taiwan
[b] Department of Chemistry, Missouri University of Science and Technology, 327 Schrenk Hall, 400 West 11th Street, Rolla, MO 65409-1120, USA
[c] Department of Laboratory Medicine and Biotechnology, Tzu Chi University, 701, Sec. 3, Zhongyang Road, Hualien 97004, Taiwan
[d] Department of Biological Sciences, Missouri University of Science and Technology, 105 Schrenk Hall, 400 West 11th Street, Rolla, MO 65409-1120, USA

ARTICLE INFO

Article history:
Received 17 March 2013
Received in revised form 9 May 2013
Accepted 26 May 2013
Available online xxx

Keywords:
Cell-penetrating peptides (CPPs)
Functionalization
Nanoparticles
Polyethylene-glycolylated (PEGylated)
Quantum dots (QDs)

ABSTRACT

Semiconductor nanoparticles, also known as quantum dots (QDs), are widely used in biomedical imaging studies and pharmaceutical research. Cell-penetrating peptides (CPPs) are a group of small peptides that are able to traverse cell membrane and deliver a variety of cargoes into living cells. CPPs deliver QDs into cells with minimal nonspecific absorption and toxic effect. In this study, water-soluble, monodisperse, carboxyl-functionalized indium phosphide (InP)/zinc sulfide (ZnS) QDs coated with polyethylene glycol lipids (designated QInP) were synthesized for the first time. The physicochemical properties (optical absorption, fluorescence and charging state) and cellular internalization of QInP and CPP/QInP complexes were characterized. CPPs noncovalently interact with QInP *in vitro* to form stable CPP/QInP complexes, which can then efficiently deliver QInP into human A549 cells. The introduction of 500 nM of CPP/QInP complexes and QInP at concentrations of less than 1 μM did not reduce cell viability. These results indicate that carboxylated and polyethylene-glycolylated (PEGylated) bifunctionalized QInP are biocompatible nanoparticles with potential for use in biomedical imaging studies and drug delivery applications.

1. Introduction

A quantum dot (QD) is composed of a few hundred to several thousand atoms, and the size of a QD typically ranges from 1 to 20 nm [1,2]. Since the first demonstration of the use of QDs as a fluorescent label in biological systems, many surface modifications and functionalizations for various applications have been described [3–5]. Due to their high photoluminescent quantum efficiency, photostability, tunability, narrow emission spectral band and prolonged fluorescence lifetime, QDs have the potential to improve sensitivity and specificity of fluoroassays relative to more traditional fluorescent proteins and organic fluorophores [2,6,7]. Many approaches have been taken to utilize QDs for biomedical imaging, including cellular labeling, intracellular sensors, deep-tissue and tumor targeting and imaging agents, and sensitizers for photothermal therapy [8]. In addition, QDs exhibit a high capacity for drug loading due to their large surface area relative to their submicron counterparts.

In general, QDs can be synthesized in aqueous solutions, nonpolar solvents or on a solid substrate [9]. A common practice is to passivate QDs with an inorganic layer of another semiconducting species with a wider band-gap, forming a core–shell structure, such as cadmium selenide (CdSe) QD cores coated with a zinc sulfide (ZnS) shell. This passivating shell provides several advantages including: (1) enhancement of QD luminescence by improving quantum yield and narrowing the emission spectrum and (2)

Abbreviations: BFP, blue fluorescent protein; CPP, cell-penetrating peptide; DMSO, dimethyl sulfoxide; DOTA, 1,4,7,10-tetraazacyclododecane-N,N′,N″,N‴-tetra acetic acid; Dox, doxorubicin; DSPE-PEG(2000), 1,2-distearoyl-sn-glycero-3-phosphoethanolamine-N-[carboxy(polyethyleneglycol)-2000]; GFP, green fluorescent protein; HR9, histidine-rich nona-arginine; MC, maurocalcine; PBS, phosphate buffered saline; PEG, polyethylene glycol; PEGylated, polyethylene-glycolylated; PEG-2-PE, 1,2-dipalmitoyl-sn-glycero-3-phosphoethanolamine-N-[methoxy(polyethyleneglycol)-2000]; QD, quantum dot; QInP, indium phosphide/zinc sulfide QDs coated with polyethylene glycol lipids; R9, nona-arginine; RFP, red fluorescent protein; Tat, transactivation of transcription; SRB, sulforhodamine B; $(TMS)_2S$, hexamethyldisilathiane; TOP, trioctylphosphine; TOPO, trioctylphosphine oxide; $ZnEt_2$, diethylzinc.

* Corresponding author. Tel.: +886 3 8633642; fax: +886 3 8633260.
** Corresponding author. Tel.: +1 573 341 6589; fax: +1 573 341 4821.
E-mail addresses: huangy@mst.edu (Y.-W. Huang), hjlee@mail.ndhu.edu.tw (H.-J. Lee).

0927-7765/$ – see front matter © 2013 Elsevier B.V. All rights reserved.
http://dx.doi.org/10.1016/j.colsurfb.2013.05.038

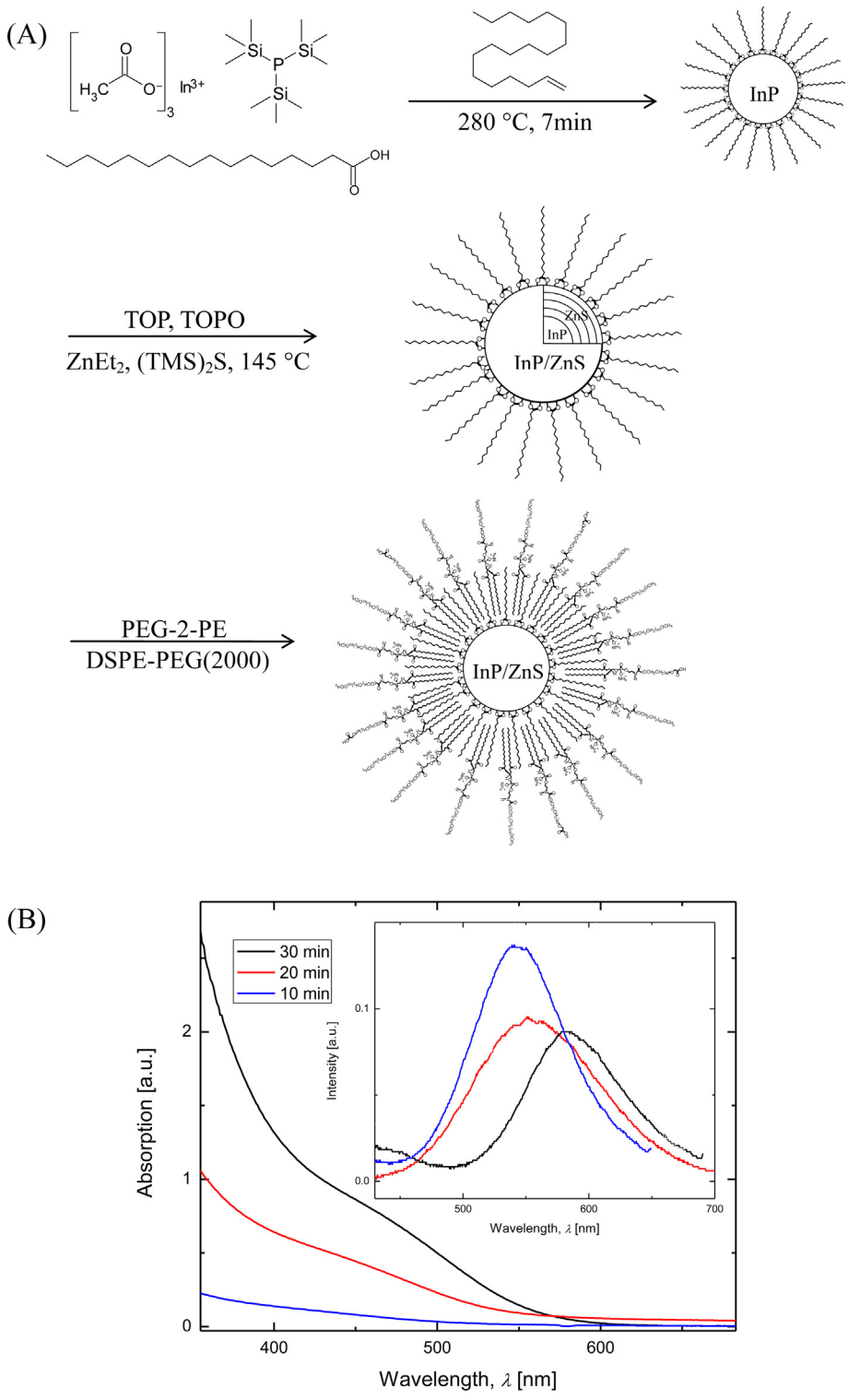

Fig. 1. Synthesis and optical characterization of carboxylated and PEGylated bifunctionalized InP/ZnS QDs (QInP). (A) Synthesis and schematic structure of QInP. TOP = trioctylphosphine, TOPO = trioctylphosphine oxide, $ZnEt_2$ = diethylzinc, $(TMS)_2S$ = hexamethyldisilathiane, PEG-2-PE = 1,2-dipalmitoyl-sn-glycero-3-phosphoethanolamine-N-[methoxy(polyethyleneglycol)-2000], DSPE-PEG(2000) = 1,2-distearoyl-sn-glycero-3-phosphoethanolamine-N-[carboxy(polyethyleneglycol)-2000]. (B) The absorption and photoluminescence (inset) spectra of QInP synthesized at 10 (blue lines), 20 (red lines), and 30 min (black lines) of reaction time. The absorption spectra of QInP were scanned using a Beckman DU 640B UV-VIS spectrophotometer, and the photoluminescence spectra of QInP were measured using a PerkinElmer LS-5 fluorescence spectrometer. (For interpretation of the references to colour in this figure legend, the reader is referred to the web version of this article.)

reduction of cytotoxicity by preventing the leaching of core materials [9,10]. The toxicity of lead sulfide (PbS) QDs can be significantly reduced by encapsulating the QD surface with polyethylene glycol (PEG) grafted (PEGylated) phospholipid micelles [11]. While QDs have been extensively studied for use in fields such as nanomedicine, the toxicity issues associated with QDs are of concern due to the unknown risks associated with biological exposure to QDs [11]. In addition, the core–shell structure can be functionalized using covalent conjugation schemes to link desired probes to the surface of the QD. The organic capping layer on the QD surface

may possess reactive groups that interact with target molecules in a covalent or noncovalent manner.

Cell-penetrating peptides (CPPs), or protein transduction domains, comprised of basic amino acid-rich sequences are able to traverse the cell membrane and deliver molecular cargoes of varied nature into living cells [12–15]. CPPs were first recognized in the human immunodeficiency virus type 1 (HIV-1) transactivation of transcription (Tat) protein that is capable of crossing plasma membranes of viral-infected and uninfected cells [16,17]. CPPs include amphipathic, hydrophobic and cationic peptides [18,19]. Research into the ability of CPPs to deliver biologically active molecules into cells has dramatically increased in recent years. CPPs are one of the most promising tools in the development of therapeutics, as evident in at least twenty medical trials [14,20]. CPP-compatible cargo molecules include proteins, nucleic acids, peptide nucleic acids, cytotoxic therapeutic drugs, inorganic particles and liposomes [13,14,21]. CPPs can deliver cargoes with sizes up to 200 nm in diameter [22]. CPPs are nontoxic to most cells and small organisms [23–27]. CPPs are also usually nontoxic *in vitro* and nonimmunogenic *in vivo* [28].

QDs do not readily enter cells, and aggregation often occurs before and after internalization [7,29]. To overcome these limitations, functionalization of the QDs surface has been performed with CPPs by either covalent [30–32] or noncovalent [33–36] linkages. CPP-facilitated delivery of QDs has the potential to reduce nonspecific absorption and adverse effects in cells and organisms [8]. We previously demonstrated that arginine-rich CPPs, such as nona-arginine (R9) and histidine-rich nona-arginine (HR9), interact with carboxylated QDs to form stably noncovalent CPP/QD complexes *in vitro* [33–36]. These CPP/QD complexes enter live cells efficiently. Furthermore, mechanistic studies revealed that the cellular uptake mechanisms of R9/QD or HR9/QD complexes involve multiple internalization pathways [33] or direct membrane translocation [36], respectively.

In this study, we (1) synthesized water-soluble, biocompatible, carboxyl- and PEG-bifunctionalized indium phosphide (InP)/ZnS QDs (QInP), (2) characterized the physicochemical properties of QInP and (3) evaluated CPP-mediated uptake of QInP into cells. The absorption and photoluminescence spectra of QInP were characterized using a spectrophotometer. The morphology and charging state of QInP and CPP/QInP complexes were characterized using an agarose-based gel retardation assay and zeta-potential analyzer. Four CPPs were used: SR9, HR9, PR9 and IR9. The intracellular delivery of CPP/QInP complexes was examined using flow cytometry, zeta-potential analysis and live cell imaging. Finally, the cytotoxicity of QInP and CPP/QInP complexes was assessed using the sulforhodamine B (SRB) assay.

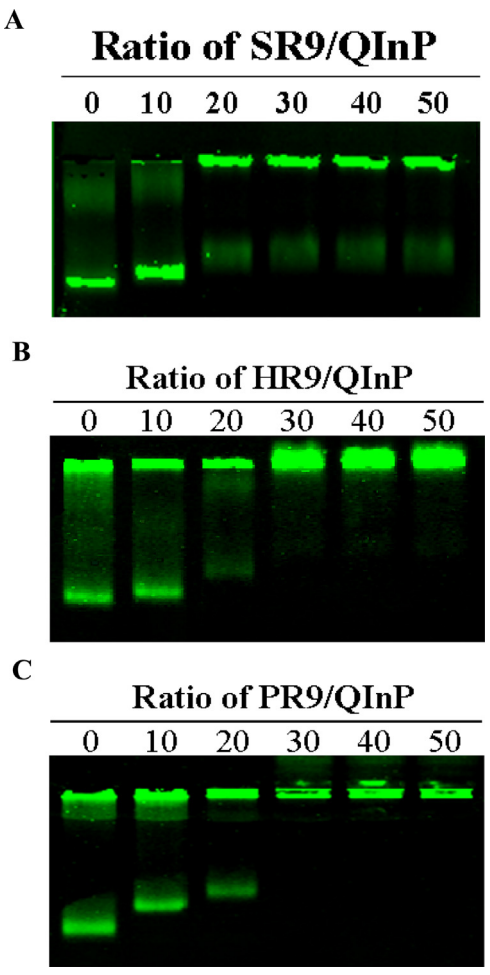

Fig. 2. Noncovalent interactions between CPPs and QInP using gel retardation assay. (A) SR9/QInP complexes. (B) HR9/QInP complexes. (C) PR9/QInP complexes. CPPs (SR9, HR9 or PR9) and QInP were incubated at molecular ratios of 0 (QInP alone), 10, 20, 30, 40 and 50. After the incubation with agitation for 2 h, the complexes were analyzed by electrophoresis on a 0.5% agarose gel. QInP fluorescence was captured using a Typhoon FLA 9000 biomolecular and Typhoon Trio imagers (GE Healthcare).

2. Materials and methods

2.1. Synthesis of InP/ZnS QDs functionalized with DSPE-PEG(2000) carboxylic acid

The preparation of QInP was based on modifications of published methods [37–40]. Indium(III) acetate and hexadecanoic acid were mixed in octadecane. Subsequently, the temperature was raised to 280 °C and tris(trimethylsilyl)phosphine was injected. Following the reaction, the flask was quickly cooled by applying compressed air, yielding InP QDs. The size and shape, which affect the optical properties of InP QDs, were controlled by modifying the reaction time. Typical reaction times were 10, 20 and 30 min A ZnS shell was added to the surface of InP QDs in the presence of trioctylphosphine (TOP), trioctylphosphine oxide (TOPO), diethylzinc (ZnEt2) and hexamethyldisilathiane ($(TMS)_2S$) at 145 °C, yielding InP/ZnS QDs. To functionalize InP/ZnS QDs with 1,2-distearoyl-sn-glycero-3-phosphoethanolamine-N-[carboxy(polyethyleneglycol)-2000] [DSPE-PEG(2000)] carboxylic acid, InP/ZnS QDs were dissolved in chloroform along with 80% (v/v) of 1,2-dipalmitoyl-sn-glycero-3-phosphoethanolamine-N-[methoxy(polyethyleneglycol)-2000] (PEG-2-PE) and 20% of DSPE-PEG(2000) carboxylic acid. The solvent was evaporated by bubbling nitrogen gas through the solution, producing a dried layer of InP/ZnS QDs and PEG lipids. The dried film was then heated to 80 °C in a water bath for several minutes, and then cooled, yielding water-soluble carboxyl-functionalized InP/ZnS QDs coated PEG lipids (denoted as QInP).

2.2. Optical characterization

Dilute solutions of QInP in deionized water were placed in 0.5 cm quartz cuvettes, and their absorption spectra were obtained using a Beckman DU 640B UV-VIS spectrophotometer (Beckman Coulter, Fullerton, CA, USA), as previously described [41]. Photoluminescence spectra were obtained using a PerkinElmer LS-5 fluorescence spectrometer (PerkinElmer, Waltham, MA, USA).

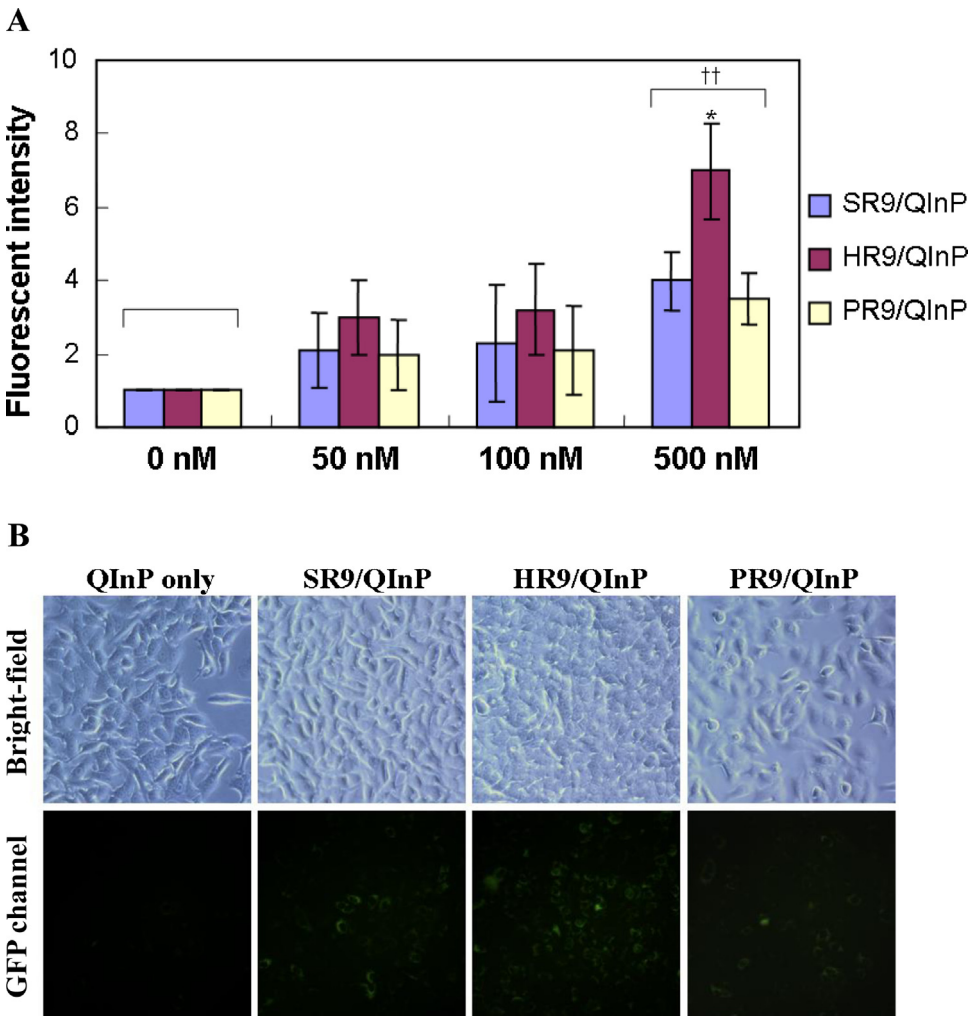

Fig. 3. Intracellular delivery of CPP/QInP complexes. (A) Fluorescent intensity of cells treated with different concentrations of CPP/QInP complexes. Cells were treated with 0 (QInP alone), 50, 100 and 500 nM CPP/QInP complexes prepared at a molecular ratio of 30 for 1 h. Each CPP/QInP complex group was compared to that of the 0 nM group. Data are presented as mean ± standard deviation from five independent experiments conducted in triplicates per treatment group. Significant differences of $P < 0.05$ (*) for individual comparison within the same group and $P < 0.01$ (††) for group comparison are indicated. (B) Microscopy of CPP-mediated QInP delivery into cells. Fifteen μM CPPs (SR9, HR9 and PR9) were mixed with 500 nM QInP to form complexes. Cells were treated with QInP alone or CPP/QInP complexes for 1 h and observed using a fluorescent microscope.

2.3. Peptide preparation

Four arginine-rich CPPs, SR9 (RRRRRRRRR), HR9 (CHHHHHRRRRRRRRRRHHHHHC), PR9 (FFLIPKGRRRRRRRRR) and IR9 (GLFEAIEGFIENGWEGMIDGWYGRRRRRRRRR), were synthesized by Genomics (Taipei, Taiwan), as previously described [23–25,36].

2.4. Gel retardation assay

To prepare CPP/QInP complexes, various amounts of CPP peptides were incubated with QInP at molecular ratios of 0 (QInP alone), 10, 20, 30, 40 and 50 in phosphate buffered saline (PBS) at 37 °C for 2 h. CPP/QInP complexes were analyzed by electrophoresis on a 0.5% agarose gel (Multi ABgarose, Thermo Fisher Scientific, Waltham, MA, USA) in 0.5 × TAE (40 mM of Tris-acetate and 1 mM of EDTA, pH 8.0) buffer at 100 V for 40 min Images were captured using a Typhoon FLA 9000 biomolecular imager (GE Healthcare, Piscataway, NJ, USA) with the excitation wavelength at 473 nm (LD laser) and the emission above 473 nm (LPB filter) [43] for SR9/QInP complexes and a Typhoon Trio imager with the excitation wavelength at 532 nm (SYAG laser) and the emission above 532 nm for HR9/QInP and PR9/QInP complexes. Data were analyzed using ImageQuant TL 7.0 software (GE Healthcare).

2.5. Cell culture

Human lung carcinoma A549 cells (American Type Culture Collection, Manassas, VA, USA; CCL-185) were maintained in Roswell Park Memorial Institute (RPMI) 1640 medium (Gibco, Invitrogen, Carlsbad, CA, USA) supplemented with 10% (v/v) bovine serum (Gibco) [33].

2.6. CPP-mediated QInP delivery into human cells

A549 cells were seeded at a density of 1×10^4 per well of 96-well plates. For the transduction of noncovalent CPP/QInP complexes, 0, 50, 100 and 500 nM of CPPs (SR9, HR9 and PR9) were mixed with QInP at a molecular ratio of 30 at 37 °C for 2 h. Without washing, CPP/QInP complexes were then incubated with cells at 37 °C for 1 h. Samples were analyzed using a flow cytometer, a Zetasizer or a confocal microscope.

2.7. Flow cytometric analysis

Cells were seeded at a density of 2.5×10^5 per well of 24-well plates. Cells in the control and experimental groups treated with QInP or CPP/QInP complexes were harvested and analyzed using a Cytomics FC500 flow cytometer (Beckman Coulter) with a FL1 filter for green fluorescent protein (GFP) detection [36].

2.8. Confocal and fluorescent microscopy

Fluorescent and bright-field images were recorded using a BD Pathway 435 bioimaging system (BD Biosciences, Franklin Lakes, NJ, USA) [36]. This system without pinhole includes both fluorescent and confocal microscopic sets. Excitation filters were at 377/50, 482/35 and 543/22 nm for blue, green and red fluorescence, respectively. Emission filters were at 435LP (long-pass), 536/40 and 593/40 nm for blue (BFP), GFP and red fluorescent protein (RFP) channels, respectively. Bright-field microscopy was used to assess cell morphology. Confocal images were also obtained using a TCS SP5 II confocal microscope system (Leica, Wetzlar, Germany). The parameters for this confocal microscopy were as follows: excitation at 405 nm and emission at 435–480 nm for the detection of BFP; excitation at 488 nm and emission at 495–540 nm for the detection of GFP; and excitation at 543 nm and emission at 590–665 nm for the detection of RFP.

2.9. Zeta-potential measurement

QInP (150 nM) or CPP/QInP complexes prepared at a molecular ratio of 30 were dissolved in double deionized water. To prepare CPP/QInP complexes, 4.5 μM of CPPs (SR9, HR9, PR9 or IR9) were mixed with 150 nM of QInP at a molecular ratio of 30 (as well as 60 for IR9) in double deionized water, and incubated at 37 °C for 2 h, as previously described [33]. Each solution was temperature-equilibrated at 25 °C for 120 s in a zeta cell. Zeta-potentials of QInP or CPP/QInP complexes were analyzed using a Zetasizer Nano ZS with Zetasizer software 6.30 (Malvern Instruments, Worcestershire, UK) [42].

2.10. Subcellular colocalization analysis

To examine subcellular localization of delivered CPP/QInP complexes, cells were treated with PBS, 500 nM of green fluorescent QInP alone or PR9/QInP complexes prepared at a molecular ratio of 30 at 37 °C for 30 min, 1 h or 2 h. Cells were washed with PBS five times to remove free PR9/QInP complexes, followed by staining with fluorescent organelle-specific trackers, as previously described [36]. Organelle trackers, 16.2 μM of Hoechst 33342 (Invitrogen; in blue) at 37 °C for 40 min and 50 nM of LysoTracker DND-99 (Invitrogen; in red) at 37 °C for 30 min (according to the manufacturer's instructions), were used to visualize subcellular colocalization in nuclei and lysosomes, respectively. Fluorescent images were detected using a BD Pathway 435 bioimaging system (BD Biosciences) or a Leica confocal microscope system (Leica).

2.11. Cytotoxicity assay

Cells were plated at a density of 1×10^4 per well in 96-well plates. Cells were treated with PBS as a negative control, treated with 100% dimethyl sulfoxide (DMSO) as a positive control, or treated with 25 nM–5 μM of QInP or 500 nM of CPP/QInP complexes prepared at a molecular ratio of 30 at 37 °C for 1 h. The cells were washed with PBS and cultured at 37 °C for 24 h. Cytotoxicity was measured by the SRB colorimetric assay [44].

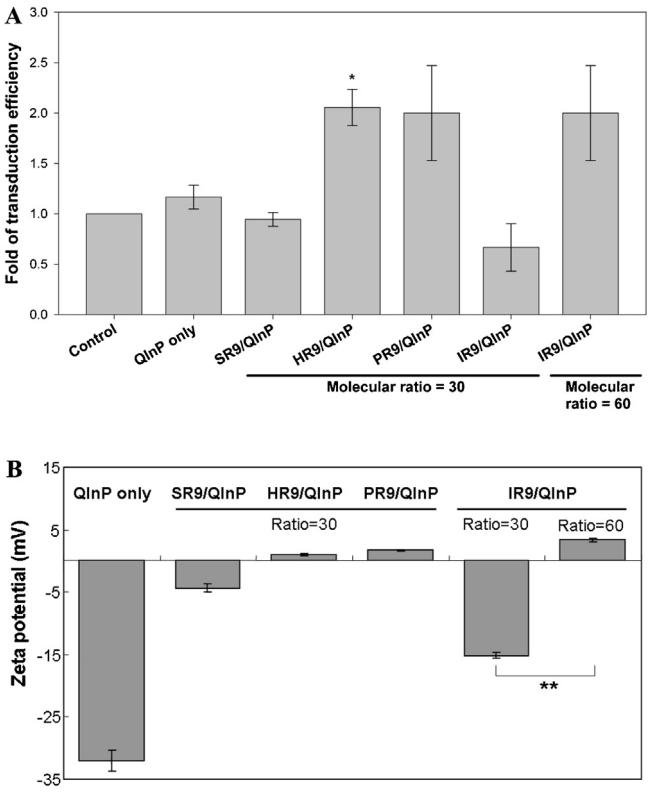

Fig. 4. Intracellular delivery and physicochemical properties of CPP/QInP complexes. (A) Flow cytometric analysis of CPP-mediated QInP delivery into A549 cells. Cells were treated with QInP alone, SR9/QInP, HR9/QInP, PR9/QInP or IR9/QInP complexes prepared at a molecular ratio of 30 or 60 for IR9/QInP complexes for 24 h, as indicated. Cells without any treatment served as the control. The fluorescent intensity and population of positive cells was analyzed using a flow cytometer. Data are presented as mean ± standard deviation from three independent experiments conducted in triplicates per treatment group. (B) Surfaced-electrical charges of different CPP/QInP complexes. SR9, HR9, and PR9 were incubated with QInP at a molecular ratio of 30, while IR9 was incubated with QInP at molecular ratios of 30 and 60. Zeta potentials of QInP and CPP/QInP complexes were determined using a Zetasizer. Data are presented as mean ± standard deviation from three independent experiments conducted in triplicates per treatment group. Significant differences were determined at $P < 0.05$ (*) and $P < 0.01$ (**).

2.12. Statistical analysis

Results are expressed as mean ± standard deviation. Mean values and standard deviations were calculated from at least three independent experiments conducted with triplicates in each treatment group. Comparisons between the control and treated groups were performed by the Student's *t*-test using levels of statistical significance of $P < 0.05$ (*, †) and 0.01 (**, ††), as indicated.

3. Results

3.1. Synthesis of carboxylated and PEGylated bifunctionalized InP/ZnS QDs

Water-soluble and carboxyl-functionalized InP/ZnS QDs were synthesized in three steps (Fig. 1A). Indium(III) acetate and tris(trimethylsilyl)phosphine were initially reacted in the presence of hexadecanoic acid and octadecane at 280 °C for 7 min in a simple one-step process. The resulting InP cores were protected with a ZnS shell, and then functionalized by PEG-2-PE and DSPE-PEG(2000) carboxylic acid. Water-soluble, PEGylated and carboxylated bifunctionalized InP/ZnS QDs were obtained (denoted as QInP).

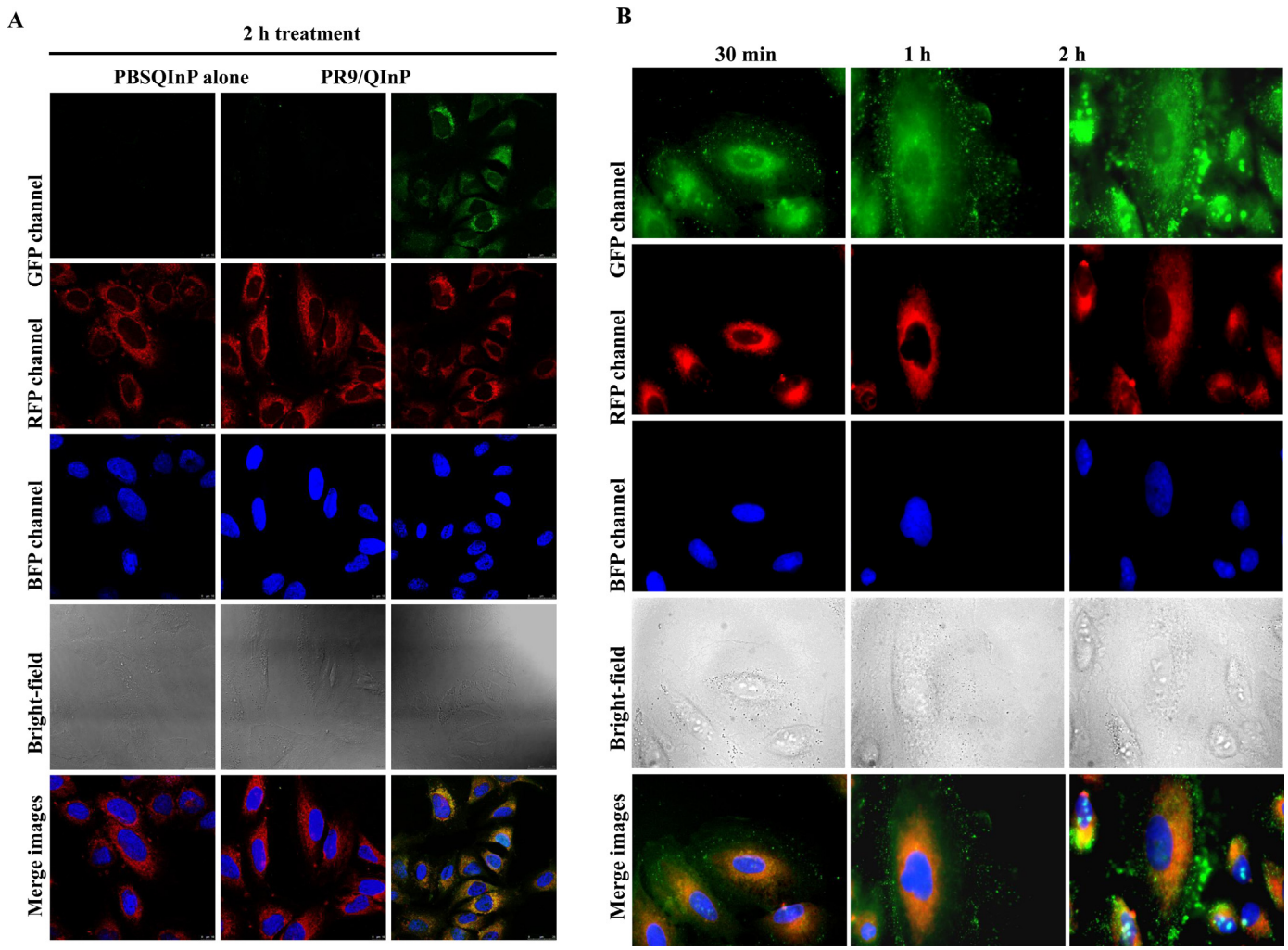

Fig. 5. Subcellular colocalization of PR9/QInP complexes. (A) Subcellular colocalization of QInP alone and PR9/QInP complexes. A549 cells were treated with PBS and QInP alone as controls or PR9/QInP complexes for 2 h, stained with LysoTracker DND-99 and Hoechst 33342, and then observed using a Leica confocal microscope system at a magnification of 600×. (B) Subcellular colocalization of PR9/QInP complexes at various time periods. A549 cells were treated with PR9/QInP complexes for 30 min, 1 h or 2 h, stained with LysoTracker DND-99 and Hoechst 33342, and then observed using a BD Pathway bioimaging system at a magnification of 600×. GFP, RFP and BFP channels displayed the distribution of QInP, lysosomes and nuclei, respectively. Overlaps between QInP and lysosomes were yellow/orange color in merged GFP and RFP images. (For interpretation of the references to colour in this figure legend, the reader is referred to the web version of this article.)

3.2. Optical characterization of QInP

The absorption spectra of QInP exhibited its first excitation peak in the range of 400–500 nm, depending on the reaction conditions employed (Fig. 1B). The photoluminescence spectra of QInP prepared at 10 min had a maximal emission peak wavelength at 525 nm. The maximal emission peak shifted to 550 and 580 nm when QInP prepared at 20 and 30 min, respectively. This red-shift in the photoluminescence correlates with an increase in particle size.

3.3. Interactions between QInP and CPPs

An agarose-based gel retardation assay was conducted to determine whether CPP forms stable complexes with QInP *in vitro*. CPPs (SR9, HR9 or PR9) were incubated with QInP at various ratios. QInP exhibited a reduced mobility when incubated with CPPs, and the mobility decreased as the concentration of CPPs increased (Fig. 2A–C). These data indicate that CPPs can interact with QInP to form stable, noncovalent complexes.

3.4. CPP-mediated intracellular delivery of QInP

To assess whether CPPs can deliver QInP into cells, human A549 cells were treated with CPP/QInP complexes prepared at a molecular ratio of 30. Green fluorescence was detected in cells treated with CPP/QInP complexes using a flow cytometer, when the concentration of QInP was above 500 nM (Fig. 3A). Using a fluorescent microscope, green fluorescence was observed in the cells treated with CPP/QInP complexes, but not in the cells treated with QInP alone (Fig. 3B). These results demonstrate that CPPs can deliver noncovalently complexed QInP into cells.

To interpret the relationship between transduction efficiency and charging state of CPP/QInP complexes, cells treated with QInP and CPP/QInP complexes were characterized using a flow cytometer, and QInP and CPP/QInP complexes were determined using a zeta-potential analyzer. Using a flow cytometer, cell population fractions with green fluorescence were detected in the cells treated with CPP/QInP complexes prepared at a molecular ratio of 30 (60 for IR9/QInP complexes) (Fig. 4A). The zeta-potential of QInP was electronegative (-32.0 ± 1.7 mV) (Fig. 4B). Zeta-potentials of CPP/QInP complexes prepared at a molecular ratio of 30 (60 for IR9/QInP

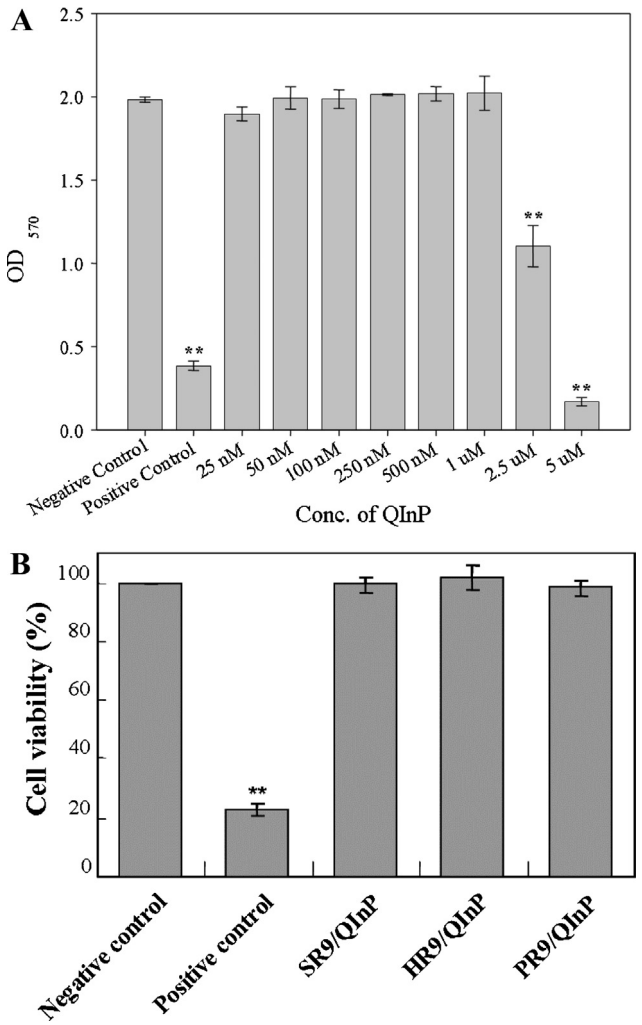

Fig. 6. Cytotoxicity of QInP and CPP/QInP complexes using the SRB assay. (A) Influence of QInP on A549 cell viability. Cells were treated with different amounts of QInP ranging from 25 nM to 5 μM. (B) Influence of CPP/QInP complexes on cell viability. Cells were treated with 500 nM CPPs (SR9, HR9 or PR9) complexed with QInP at a molecular ratio of 30. Cells without any treatment served as a negative control, and cells treated with 100% DMSO were served as a positive control. Each group is compared with the negative control, and significant differences of $P < 0.01$ (**) are indicated. Data are presented as mean ± standard deviation from three independent experiments conducted in triplicates per treatment group.

complexes) were more electropositive. These data indicate that charging state of CPP/QInP complexes correlate with transduction efficiency.

To reveal subcellular localization of CPP/QInP complexes, cells were treated with PBS, QInP or PR9/QInP complexes and stained with organelle-specific fluorescent markers LysoTracker DND-99 and Hoechst 33342 for the visualization of lysosomes and nuclei, respectively. The majority of QInP distributed evenly in the cytosol following PR9-mediated delivery (Fig. 5A and B). The merged images revealed that QInP colocalized with lysosomes in most cells after transduction delivery. This result is consistent with our previous finding that endocytosis is the main route for intracellular delivery of PR9/cargo complexes (manuscript submitted).

3.5. Cytotoxicity of CPP/QInP complexes

To determine the effect of QInP and CPP/QInP complexes on cell viability, the SRB assay was performed. QInP had no significant effect on cell viability at or below 1 μM (Fig. 6A), while 500 nM of CPPs (SR9, HR9 or PR9) complexed with QInP at a molecular ratio of 30 were not cytotoxic (Fig. 6B). We have previously demonstrated that QDs and CPP/QD complexes are not toxic to A549 cells by the SRB assay [33,36].

4. Discussion

The novel physicochemical characteristics give semiconductor QDs specific advantages in certain research and medical applications [45]. Potentially the most important application of QDs is their use as diagnostic and therapeutic tools in nanomedicine [45]. In this study, we synthesized novel water-soluble, PEGylated and carboxyl-functionalized InP/ZnS QDs. Their physicochemical properties, including optical features, morphology and charging state, and cellular internalization of QInP and CPP/QInP complexes were characterized. We found that CPPs can deliver noncovalently complexed QInP into live cells. PR9/QInP complexes were localized in lysosomes. This is consistent with the notion that endocytosis is the major route for cellular entry. Finally, cell viability assays showed that CPP/QInP complexes were not cytotoxic when 500 nM of CPP was complexed with QInP at a molecular ratio of 30, and QInP did not result in significant cytotoxicity when the concentrations were at or less than 1 μM.

Functionalized nanoparticles have become key players for enhancing the contrast of images in molecular imaging and medical diagnostics [46]. Since the late 1980s, a large number of binary III-V materials, such as gallium phosphide (GaP) and InP, exhibiting infrared bandgaps as bulk semiconductors, were prepared as solution-based nanocrystals [47]. Many research teams have been using cadmium-free QDs, such as InP, to address concerns about cadmium cytotoxicity [48]. One key advantage offered by InP QDs lies in the robustness of the covalent bond in III-V semiconductors *versus* the ionic bond in the II-VI semiconductors and, thus, reduced toxicity. InP QDs with promising size-tunable emission in the near-infrared and visible range have emerged as a replacement for cadmium-based QDs [49]. However, reports on colloidal synthesis of InP QDs are few, and size homogeneity has been limited [49]. Nag and Sarma reported an efficient and fast solvothermal route to prepare InP QDs [50]. This method used a reaction temperature as high as 430 °C, accelerating the reaction.

A ZnS shell on the surface of solvothermal synthesized InP QDs could be surface-modified with hydrophilic ligands in an aqueous solution at room temperature [51]. The resulting InP/ZnS QDs exhibit enhanced luminescent efficiency relative to InP QDs. The ZnS shells serve two purposes: (1) improving the quantum yield by passivating the surface nonradiative recombination sites and (2) acting as a barrier between the inorganic core and the surrounding solvent, thereby preventing the leakage of unwanted ions [52]. Chibli et al. reported survival assays in five cell lines, and showed a distinct reduction in toxicity with the double-shell InP QDs, compared to a single ZnS shell [49]. These results indicated that InP QDs could be an effective alternative to cadmium-containing QDs. Recently, large-scale synthesis of InP/ZnS QDs was conducted in a hybrid flow reactor that combined a batch-type mixer with a flow-rate furnace in a simple one-step process [53]. The same group also reported that uniform, large InP/ZnS QDs could be produced using a newly synthesized organometallic phosphorus (P) precursor, tris(tert-butyldimethylsilyl)phosphine, and a low temperature regime (210–300 °C) [54]. Large-area freestanding films of InP/ZnS QDs over 50 cm × 50 cm were recently reported [55].

Surface functionalization of amphipathic InP QDs with folate rendered endocytosis of folate receptor-mediated delivery of InP QDs in folate-receptor-positive KB cells [52]. Gao et al. reported that InAs/InP/ZnSe QDs functionalized with mercaptopropionic acid (MPA) accumulated in the tumor area of nude mice bearing 22B or LS174T tumors [56]. Furthermore, InAs/InP/ZnSe QDs

functionalized with the arginine-glycine-aspartic acid (RGD) tripeptide could be recognized by the cell adhesion molecule integrin $\alpha_v\beta_3$, a key player in tumor angiogenesis, progression and spread [57]. Recently, dendron- and dendron-$(RGD)_2$-functionalized InP QDs have been introduced as translatable nanoprobes for clinical imaging applications [58]. Dendron-coated InP/ZnS QDs lacked significant toxicity at exposure doses of 1 μg InP/g mouse weight. These InP QDs exhibited important features, including high stability, biocompatibility, near-infrared emission and nontoxicity. Comparisons were also been made between doxorubicin (Dox)-functionalized gold (Au) nanoparticles and Dox-functionalized InP QDs as tools for therapeutic effectiveness [59]. Our InP QDs had no effect on cell viability at or below 1 μM. In the future, QInP can be functionalized with activatable cell-penetrating peptides (ACPPs) to inhibit target gene expression by RNA interference (RNAi) for biological applications.

There have been few investigations on the use of CPPs with InP QDs. Rosenberg et al. functionalized InP/ZnS QDs with CAAKATat CPPs, forming QD-CAAKATat-DOTA-Dy, where DOTA and Dy are 1,4,7,10-tetraazacyclododecane-N,N′,N″,N‴-tetra acetic acid and dysprosium^{3+}, respectively [60]. They found that QD-CAAKATat-DOTA-Dy were located in vesicular compartments, and were not cytotoxic to Chinese hamster ovary (CHO) cells. The incorporation of Tat peptide provided effective self-transfecting properties. Stasiuk et al. reported functionalization of InP/ZnS QDs with mauro-calcine (MC) CPPs from scorpion toxin [46]. Fluorescent MC-InP QDs showed cellular internalization with bright magnetic resonance imaging signal, and increased tissue retention time. Our present study reveals the utility of three additional kinds of arginine-rich CPPs to deliver QInP for biological applications.

5. Conclusions

We synthesized and characterized carboxylated and PEGylated bifunctionalized InP/ZnS QDs (QInP). CPPs (SR9, HR9, PR9 and IR9) were able to deliver noncovalently complexed QInP into human A549 cells. These results indicate that bifunctionalized QInP may be an excellent biocompatible tool for biomedical imaging and drug delivery applications. Notably, the present synthetic protocol of QInP could be easily extended to produce additional functionalized QDs as multimodal imaging agents in the future.

Acknowledgments

We are grateful to Chia-Liang Cheng (Department of Physics, National Dong Hwa University, Taiwan) for performing the zeta-potential measurements, and Core Instrument Center (National Health Research Institutes, Miaoli, Taiwan) for the Typhoon Trio imager and Leica TCS SP5 II confocal system. This work was supported by the Postdoctoral Fellowship NSC 101-2811-B-259-001 (to B.R. Liu) and the Grant Number NSC 101-2320-B-259-002-MY3 from the National Science Council of Taiwan (to H.-J. Lee).

References

[1] A.P. Alivisatos, Semiconductor clusters, nanocrystals, and quantum dots, Science 271 (1996) 933–937.
[2] H. Mattoussi, G. Palui, H.B. Na, Luminescent quantum dots as platforms for probing *in vitro* and *in vivo* biological processes, Adv. Drug Deliv. Rev. 64 (2012) 138–166.
[3] K.T. Yong, Quantum dots for biophotonics, Theranostics 2 (2012) 629–630.
[4] M. Bruchez, M. Moronne, P. Gin, S. Weiss, A.P. Alivisatos, Semiconductor nanocrystals as fluorescent biological labels, Science 281 (1998) 2012–2016.
[5] W.C.W. Chan, S. Nie, Quantum dot bioconjugates for ultrasensitive nonisotopic detection, Science 281 (1998) 2016–2018.
[6] F. Chen, D. Gerion, Fluorescent CdSe/ZnS nanocrystal-peptide conjugates for long-term, nontoxic imaging and nuclear targeting in living cells, Nano Lett. 4 (2004) 1827–1832.
[7] X. Michalet, F.F. Pinaud, L.A. Bentolila, J.M. Tsay, S. Doose, J.J. Li, G. Sundaressan, A.M. Wu, S.S. Gambhir, S. Weiss, Quantum dots for live cells, *in vivo* imaging, and diagnostics, Science 307 (2005) 538–544.
[8] L. Shao, Y. Gao, F. Yan, Semiconductor quantum dots for biomedical applications, Sensors 11 (2011) 11736–11751.
[9] Y. Zhang, T.H. Wang, Quantum dot enabled molecular sensing and diagnostics, Theranostics 2 (2012) 631–654.
[10] P.M. Farias, B.S. Santos, A. Fontes, Semiconductor fluorescent quantum dots: efficient biolabels in cancer diagnostics, Methods Mol. Biol. 544 (2009) 407–419.
[11] R. Hu, W.C. Law, G. Lin, L. Ye, J. Liu, J. Liu, L. Reynolds, K.T. Yong, PEGylated phospholipid micelle-encapsulated near-infrared PbS quantum dots for in vivo and in vitro bioimaging, Theranostics 2 (2012) 723–733.
[12] F. Madani, S. Lindberg, U. Langel, S. Futaki, A. Graslund, Mechanisms of cellular uptake of cell-penetrating peptides, J. Biophys. 2011 (2011) 414729.
[13] I. Mager, K. Langel, T. Lehto, E. Eiriksdottir, U. Langel, The role of endocytosis on the uptake kinetics of luciferin-conjugated cell-penetrating peptides, Biochim. Biophys. Acta 1818 (2012) 502–511.
[14] A. van den Berg, S.F. Dowdy, Protein transduction domain delivery of therapeutic macromolecules, Curr. Opin. Biotechnol. 22 (2011) 888–893.
[15] N. Schmidt, A. Mishra, G.H. Lai, G.C. Wong, Arginine-rich cell-penetrating peptides, FEBS Lett. 584 (2010) 1806–1813.
[16] M. Green, P.M. Loewenstein, Autonomous functional domains of chemically synthesized human immunodeficiency virus Tat trans-activator protein, Cell 55 (1988) 1179–1188.
[17] A.D. Frankel, C.O. Pabo, Cellular uptake of the Tat protein from human immunodeficiency virus, Cell 55 (1988) 1189–1193.
[18] K.M. Wagstff, D.A. Jans, Protein transduction: cell penetrating peptides and their therapeutic applications, Curr. Med. Chem. 13 (2006) 1371–1387.
[19] A. Gautam, H. Singh, A. Tyagi, K. Chaudhary, R. Kumar, P. Kapoor, G.P. Raghava, CPPsite: a curated database of cell penetrating peptides, Database 2012 (2012) bas015.
[20] I. Nakase, Y. Konishi, M. Ueda, H. Saji, S. Futaki, Accumulation of arginine-rich cell-penetrating peptides in tumors and the potential for anticancer drug delivery *in vivo*, J. Control. Release 159 (2012) 181–188.
[21] J.M. Gump, S.F. Dowdy, Tat transduction: the molecular mechanism and therapeutic prospects, Trends Mol. Med. 13 (2007) 443–448.
[22] J.S. Wadia, S.F. Dowdy, Protein transduction technology, Curr. Opin. Biotechnol. 13 (2002) 52–56.
[23] Y.H. Dai, B.R. Liu, H.J. Chiang, H.J. Lee, Gene transport and expression by arginine-rich cell-penetrating peptides in *Paramecium*, Gene 489 (2011) 89–97.
[24] Y.J. Chen, B.R. Liu, Y.H. Dai, C.Y. Lee, M.H. Chan, H.H. Chen, H.J. Chiang, H.J. Lee, A gene delivery system for insect cells mediated by arginine-rich cell-penetrating peptides, Gene 493 (2012) 201–210.
[25] B.R. Liu, M.D. Lin, H.J. Chiang, H.J. Lee, Arginine-rich cell-penetrating peptides deliver gene into living human cells, Gene 505 (2012) 37–45.
[26] G. Tunnemann, G. Ter-Avetisyan, R.M. Martin, M. Stockl, A. Herrmann, M.C. Cardoso, Live-cell analysis of cell penetration ability and toxicity of oligo-arginines, J. Pept. Sci. 14 (2008) 469–476.
[27] K. Kilk, R. Mahlapuu, U. Soomets, U. Langel, Analysis of *in vitro* toxicity of five cell-penetrating peptides by metabolic profiling, Toxicology 265 (2009) 87–95.
[28] J. Suhorustsenko, N. Oskolkov, P. Arukuusk, K. Kurrikoff, E. Eriste, D.M. Copolovici, U. Langel, Cell-penetrating peptides, PepFects, show no evidence of toxicity and immunogenicity *in vitro* and *in vivo*, Bioconjug. Chem. 22 (2011) 2255–2262.
[29] J.B. Delehanty, H. Mattoussi, I.L. Medintz, Delivering quantum dots into cells: strategies, progress and remaining issues, Anal. Bioanal. Chem. 393 (2009) 1091–1105.
[30] F.L. Xue, J.Y. Chen, J. Guo, C.C. Wang, W.L. Yang, P.N. Wang, D.R. Lu, Enhancement of intracellular delivery of CdTe quantum dots (QDs) to living cells by Tat conjugation, J. Fluoresc. 17 (2007) 149–154.
[31] Y.E. Koshman, S.B. Waters, L.A. Walker, T. Los, P. de Tombe, P.H. Goldspink, B. Russell, Delivery and visualization of proteins conjugated to quantum dots in cardiac myocytes, J. Mol. Cell. Cardiol. 45 (2008) 853–856.
[32] Y. Wei, N.R. Jana, S.J. Tan, J.Y. Ying, Surface coating directed cellular delivery of Tat-functionalized quantum dots, Bioconjug. Chem. 20 (2009) 1752–1758.
[33] B.R. Liu, J.F. Li, S.W. Lu, H.J. Lee, Y.W. Huang, K.B. Shannon, R.S. Aronstam, Cellular internalization of quantum dots noncovalently conjugated with arginine-rich cell-penetrating peptides, J. Nanosci. Nanotech. 10 (2010) 6534–6543.
[34] B.R. Liu, Y.W. Huang, H.J. Chiang, H.J. Lee, Cell-penetrating peptide-functionized quantum dots for intracellular delivery, J. Nanosci. Nanotechnol. 10 (2010) 7897–7905.
[35] Y. Xu, B.R. Liu, H.J. Lee, K.B. Shannon, J.G. Winiarz, T.C. Wang, H.J. Chiang, Y.W. Huang, Nona-arginine facilitates delivery of quantum dots into cells via multiple pathways, J. Biomed. Biotechnol. 2010 (2010) 948543.
[36] B.R. Liu, Y.W. Huang, J.G. Winiarz, H.J. Chiang, H.J. Lee, Intracellular delivery of quantum dots mediated by a histidine- and arginine-rich HR9 cell-penetrating peptide through the direct membrane translocation mechanism, Biomaterials 32 (2011) 3520–3537.
[37] N. Depalo, A. Mallardi, R. Comparelli, M. Striccoli, A. Agostiano, M.L. Curri, Luminescent nanocrystals in phospholipid micelles for bioconjugation: an optical and structural investigation, J. Colloid Interface Sci. 325 (2008) 558–566.
[38] Y. Shi, P. He, X. Zhu, Photoluminescence-enhanced biocompatible quantum dots by phospholipid functionalization, Mater. Res. Bull. 43 (2008) 2626–2635.

[39] J.A. Gerbec, D. Magana, A. Washington, G.F. Strouse, Microwave-enhanced reaction rates for nanoparticle synthesis, J. Am. Chem. Soc. 127 (2005) 15791–15800.
[40] B.O. Dabbousi, J. Rodriguez-Viejo, F.V. Mikulec, J.R. Heine, H. Mattoussi, R. Ober, K.F. Jensen, M.G. Bawendi, (CdSe)ZnS core-shell quantum dots: synthesis and characterization of a size series of highly luminescent nanocrystallites, J. Phys. Chem. B 101 (1997) 9463–9475.
[41] T.M. Fears, C. Anderson, J.G. Winiarz, Photorefractivity in a polymeric composite photosensitized with NiS nanocrystals, J. Chem. Phys. 129 (2008) 154704.
[42] B.R. Liu, H.J. Chiang, Y.W. Huang, M.H. Chan, H.H. Chen, H.J. Lee, Cellular internalization of quantum dots mediated by cell-penetrating peptides, Pharm. Nanotechnol. 1 (2013) 151–161.
[43] J.S. Liou, B.R. Liu, A.L. Martin, Y.W. Huang, H.J. Chiang, H.J. Lee, Protein transduction in human cells is enhanced by cell-penetrating peptides fused with an endosomolytic HA2 sequence, Peptides 37 (2012) 273–284.
[44] J.W. Hu, B.R. Liu, C.Y. Wu, S.W. Lu, H.J. Lee, Protein transport in human cells mediated by covalently and noncovalently conjugated arginine-rich intracellular delivery peptides, Peptides 30 (2009) 1669–1678.
[45] M.J.D. Clift, V. Stone, Quantum dots: an insight and perspective of their biological interaction and how this relates to their relevance for clinical use, Theranostics 2 (2012) 668–680.
[46] G.J. Stasiuk, S. Tamang, D. Imbert, C. Poillot, M. Giardiello, C. Tisseyre, E.L. Barbier, P.H. Fries, M. de Waard, P. Reiss, M. Mazzanti, Cell-permeable Ln(III) chelate-functionalized InP quantum dots as multimodal imaging agents, ACS Nano 5 (2011) 8193–8201.
[47] A.L. Rogach, A. Eychmuller, S.G. Hickey, S.V. Kershaw, Infrared-emitting colloidal nanocrystals: synthesis, assembly, spectroscopy, and applications, Small 3 (2007) 536–557.
[48] K.T. Young, Y. Wang, I. Roy, H. Rui, M.T. Swihart, W.C. Law, S.K. Kwak, L. Ye, J. Liu, S.D. Mahajan, J.L. Reynolds, Preparation of quantum dot/drug nanoparticles formulations for traceable targeted delivery and therapy, Theranostics 2 (2012) 681–694.
[49] H. Chibli, L. Carlini, S. Park, N.M. Dimitrijevic, J.L. Nadeau, Cytotoxicity of InP/ZnS quantum dots related to reactive oxygen species generation, Nanoscale 3 (2011) 2552–2559.
[50] A. Nag, D.D. Sarma, Solvothermal synthesis of InP quantum dots, J. Nanosci. Nanotechnol. 9 (2009) 5633–5636.
[51] H.J. Byun, J.C. Lee, H. Yang, Solvothermal synthesis of InP quantum dots and their enhanced luminescent efficiency by post-synthetic treatments, J. Colloid Interface Sci. 355 (2011) 35–41.
[52] D.J. Bharali, D.W. Lucey, H. Jayakumar, H.E. Pudavar, P.N. Prasad, Folate-receptor-mediated delivery of InP quantum dots for bioimaging using confocal and two-photon microscopy, J. Am. Chem. Soc. 127 (2005) 11364–11371.
[53] K. Kim, S. Jeong, J.Y. Woo, C.S. Han, Successive and large-scale synthesis of InP/ZnS quantum dots in a hybrid reactor and their application to white LEDs, Nanotechnology 23 (2012) 065602.
[54] S. Joung, S. Yoon, C.S. Han, Y. Kim, S. Jeong, Facile synthesis of uniform large-sized InP nanocrystal quantum dots using tris(tert-butyldimethylsilyl)phosphine, Nanoscale Res. Lett. 7 (2012) 93.
[55] E. Mutlugun, P.L. Hernandez-Martinez, C. Eroglu, Y. Coskun, T. Erdem, V.K. Sharma, E. Unal, S.K. Hickey, N. Gaponik, A. Eychmuller, H.V. Demir, Large-area (over 50 cm × 50 cm) freestanding films of colloidal InP/ZnS quantum dots, Nano Lett. 12 (2012) 3986–3993.
[56] J. Gao, K. Chen, R. Xie, J. Xie, S. Lee, Z. Cheng, X. Peng, X. Chen, Ultrasmall near-infrared non-cadmium quantum dots for in vivo tumor imaging, Small 6 (2010) 256–261.
[57] J. Gao, K. Chen, R. Xie, J. Xie, Y. Yan, Z. Cheng, X. Peng, X. Chen, In vivo tumor-targeted fluorescence imaging using near-infrared non-cadmium quantum dots, Bioconjug. Chem. 21 (2010) 604–609.
[58] J. Gao, K. Chen, R. Luong, D.M. Bouley, H. Mao, T. Qiao, S.S. Gambhir, Z. Cheng, A novel clinically translatable fluorescent nanoparticles for targeted molecular imaging of tumors in living subjects, Nano Lett. 12 (2012) 281–286.
[59] X. Zhang, H. Chibli, D. Kong, J. Nadeau, Comparative cytotoxicity of gold-doxorubicin and InP-doxorubicin conjugates, Nanotechnology 23 (2012) 275103.
[60] J.T. Rosenberg, J.M. Kogot, D.D. Lovingood, G.F. Strouse, S.C. Grant, Intracellular bimodal nanoparticles based on quantum dots for high-field MRI at 21.1 T, Magn. Reson. Med. 64 (2010) 871–882.